Measurement and modeling of ultrafast carrier dynamics and transport in germanium/silicon-germanium quantum wells

Stephanie A. Claussen,[1,3,*] Emel Tasyurek,[1,3] Jonathan E. Roth, [1,2] and David A. B. Miller[1]

[1]*Edward L. Ginzton Laboratory, Stanford University, 348 Via Pueblo Mall, Stanford, CA 94305, USA*
[2]*Currently with Aurrion, LLC, 5385 Hollister Ave #207, Santa Barbara, CA 93111, USA*
[3]*These authors contributed equally to this work.*
**sclaussen@stanford.edu*

Abstract: We measure the intervalley scattering time of electrons in the conduction band of Ge quantum wells from the direct Γ valley to the indirect L valley to be ~185 fs using a pump-probe setup at 1570 nm. We relate this to the width of the exciton peak seen in the absorption spectra of this material, and show that these quantum wells could be used as a fast saturable absorber with a saturation fluence between 0.11 and 0.27 pJ/μm^2. We also observe field screening by photogenerated carriers in the material on longer timescales. We model this field screening by incorporating carrier escape from the quantum wells, drift across the intrinsic region, and recovery of the applied voltage through diffusive conduction.

OCIS codes: (230.0250) Optoelectronics; (230.4205) Multiple quantum well (MQW) modulators; (320.2250) Femtosecond phenomena; (200.4650) Optical interconnects; (230.5590) Quantum-well, -wire and -dot devices.

References and links

1. Y.-H. Kuo, Y. K. Lee, Y. Ge, S. Ren, J. E. Roth, T. I. Kamins, D. A. B. Miller, and J. S. Harris, Jr., "Quantum-Confined Stark Effect in Ge/SiGe Quantum Wells on Si for Optical Modulators," IEEE J. Sel. Top. Quantum Electron. **12**(6), 1503–1513 (2006).
2. J. E. Roth, O. Fidaner, R. K. Schaevitz, Y.-H. Kuo, T. I. Kamins, J. S. Harris, and D. A. B. Miller, "Optical modulator on silicon employing germanium quantum wells," Opt. Express **15**(9), 5851–5859 (2007), http://www.opticsinfobase.org/abstract.cfm?URI=oe-15-9-5851.
3. J. E. Roth, O. Fidaner, E. H. Edwards, R. K. Schaevitz, Y.-H. Kuo, N. C. Helman, T. I. Kamins, J. S. Harris, and D. A. B. Miller, "C-band side-entry Ge quantum-well electroabsorption modulator on SOI operating at 1 V swing," Electron. Lett. **44**(1), 49–50 (2008).
4. J. Shah, *Ultrafast Spectroscopy of Semiconductors and Semiconductor Nanostructures* (Springer-Verlag, Berlin, 1999).
5. G. Mak, H. M. van Driel, "Femtosecond transmission spectroscopy at the direct band edge of germanium," Phys. Rev. B Condens. Matter **49**(23), 16817–16820 (1994).
6. X. Zhou, H. van Driel, and G. Mak, "Femtosecond kinetics of photoexcited carriers in germanium," Phys. Rev. B Condens. Matter **50**(8), 5226–5230 (1994).
7. C. Lange, N. S. Koster, S. Chatterjee, H. Sigg, D. Chrastina, G. Isella, H. von Kanel, B. Kunert, and W. Stolz, "Comparison of ultrafast carrier thermalization in $Ga_xIn_{1-x}As$ and Ge quantum wells," Phys. Rev. B **81**(4), 045320 (2010).
8. S. Claussen, L. Tang, J. Roth, O. Fidaner, S. Latif, and D. A. B. Miller, "Femtosecond carrier dynamics in Ge/SiGe quantum wells," presented at the 4th International Conference on Group IV Photonics, Tokyo, Japan, 19–21 Sept. 2007.
9. J. A. Cavaillès, D. A. B. Miller, J. E. Cunningham, P. L. Kam Wa, and A. Miller, "Simultaneous measurement of electron and hole escape times from biased single quantum wells," Appl. Phys. Lett. **61**(4), 426–428 (1992).
10. G. Livescu, D. A. B. Miller, T. Sizer, D. J. Burrows, J. Cunningham, A. C. Gossard, and J. H. English, "High-speed absorption recovery in quantum well diodes by diffusive electrical conduction," Appl. Phys. Lett. **54**(8), 748–750 (1989).
11. M. B. Yairi, and D. A. B. Miller, "Equivalence of diffusive conduction and giant ambipolar diffusion," J. Appl. Phys. **91**(7), 4374–4381 (2002).

#136041 - $15.00 USD Received 4 Oct 2010; revised 11 Nov 2010; accepted 14 Nov 2010; published 22 Nov 2010

12. H. S. Wang, F. J. Effenberger, P. LiKamWa, and A. Miller, "Ultrafast cross-well carrier transport in a strained multiple-quantum-well InGaAs-GaAs p-i-n modulator," IEEE J. Quantum Electron. **33**(2), 192–197 (1997).
13. R. K. Schaevitz, J. E. Roth, S. Ren, O. Fidaner, and D. A. B. Miller, "Material Properties in Si-Ge/Ge Quantum Wells," IEEE J. Sel. Top. Quantum Electron. **14**(4), 1082–1089 (2008).
14. D. T. Reid, "Measuring ultra fast laser pulses," in *Ultrafast Photonics*, A. Miller, D.T. Reid, and D.M. Finlayson, ed. (Bristol and Philadelphia: Scottish Universities Summer School in Physics and Institute of Physics Publishing, 2002).
15. A. Othonos, "Probing ultrafast carrier and phonon dynamics in semiconductors," J. Appl. Phys. **83**(4), 1789–1830 (1998).
16. M. V. Lebedev, O. V. Misochko, T. Dekorsy, and N. Georgiev, "On the nature of "coherent artifact"," J. Exp. Theor. Phys. **100**(2), 272–282 (2005).
17. A. E. Siegman, M. W. Sasnett, and T. F. Johnston, "Choice of Clip Levels for Beam Width Measurements Using Knife-Edge Techniques," IEEE J. Quantum Electron. **27**(4), 1098–1104 (1991).
18. E. R. Brown, D. C. Driscoll, and A. C. Gossard, "State-of-the-art in 1.55 μm ultrafast InGaAs photoconductors, and the use of signal processing techniques to extract the photocarrier lifetime," Semicond. Sci. Technol. **20**(7), 199–204 (2005).
19. D. S. Chemla, D. A. B. Miller, P. W. Smith, A. C. Gossard, and W. Wiegmann, "Room Temperature Excitonic Nonlinear Absorption and Refraction in GaAs/AlGaAs Multiple Quantum Well Structures," IEEE J. Quantum Electron. **20**(3), 265–275 (1984).
20. E. H. Edwards, R. M. Audet, Y. Rong, S. A. Claussen, R. K. Schaevitz, E. Tasyürek, S. Ren, and I. Ted, Kamins, O. I. Dosunmu, M. S. Ünlu, J. S. Harris, and D. A. B. Miller, "Si-Ge Surface-normal Asymmetric Fabry-Perot Quantum-confined Stark Effect Electroabsorption Modulator," presented at the IEEE Annual Photonics Society Meeting, Denver, CO, 7–11 Nov. 2010.
21. P. Chaisakul, D. Marris-Morini, G. Isella, D. Chrastina, X. Le Roux, E. Gatti, S. Edmond, J. Osmond, E. Cassan, and L. Vivien, "Quantum-confined Stark effect measurements in Ge/SiGe quantum-well structures," Opt. Lett. **35**(17), 2913–2915 (2010).
22. J. Roth, "Electroabsorption Modulators for CMOS Compatible Optical Interconnects in III-V and Group IV Materials," Stanford University Electrical Engineering Ph.D. Dissertation, August 2007.
23. F. J. Grawert, J. T. Gopinath, F. Ö. Ilday, H. M. Shen, E. P. Ippen, F. X. Kärtner, S. Akiyama, J. Liu, K. Wada, and L. C. Kimerling, "220-fs erbium-ytterbium:glass laser mode locked by a broadband low-loss silicon/germanium saturable absorber," Opt. Lett. **30**(3), 329–331 (2005).
24. Y. Silberberg, P. W. Smith, D. J. Eilenberger, D. A. B. Miller, A. C. Gossard, and W. Wiegmann, "Passive mode locking of a semiconductor diode laser," Opt. Lett. **9**(11), 507–509 (1984).
25. U. Keller, D. A. B. Miller, G. D. Boyd, T. H. Chiu, J. F. Ferguson, and M. T. Asom, "Solid-state low-loss intracavity saturable absorber for Nd:YLF lasers: an antiresonant semiconductor Fabry-Perot saturable absorber," Opt. Lett. **17**(7), 505–507 (1992).
26. M. A. Omar, and L. Reggiani, "Drift velocity and diffusivity of hot carriers in germanium: model calculations," Solid-State Electron. **30**(12), 1351–1354 (1987).

1. Introduction

A detailed understanding of the carrier dynamics and transport properties of semiconductor optoelectronic materials is necessary to design and optimize high-performance devices. Ge/SiGe quantum wells (QWs) are of particular current interest, as this material system exhibits the quantum-confined Stark effect (QCSE) [1], a strong, high-speed electroabsorption effect that enables compact, low-energy, CMOS-compatible optical modulators [2,3]. Up to this point, little work has been done to investigate the ultrafast dynamics of Ge/SiGe QWs. Of particular importance to device performance are changes that occur on timescales ranging from hundreds of femtoseconds—usually caused by carrier scattering [4]—to tens of picoseconds, during which carrier transport occurs across the active region of devices.

Measurements of femtosecond carrier dynamics have been carried out previously in Ge-based materials. Prior work set an upper limit of 230 fs on the scattering time of electrons in the conduction band from the direct Γ valley to the indirect L valley in bulk Ge using both time-resolved transmission and luminescence up-conversion experiments [5,6]. More recently, Ge/SiGe QWs have been investigated [7], with evidence found of a femtosecond transient population inversion. We also previously briefly reported preliminary measurements of this fast scattering behavior in Ge QWs [8].

Extensive work has been done on carrier transport in QW *p-i-n* diodes. The influence of photogenerated carriers on the absorption characteristics of QWs was explained using two primary mechanisms: excitonic saturation and carrier screening of the applied electric field

#136041 - $15.00 USD Received 4 Oct 2010; revised 11 Nov 2010; accepted 14 Nov 2010; published 22 Nov 2010

[9]. Based on the prior findings just described for bulk Ge, in our work we expect the dominant excitonic saturation to be due to filling of the available states in the direct Γ valley of the conduction band in the Ge wells, with subsequent recovery due to intervalley scattering to the indirect L valley. The field screening due to the movement of photogenerated carriers towards the biasing electrodes leads to absorption changes that can relax very quickly through "diffusive conduction" [10,11], a two-dimensional, lateral mechanism which has been included in models of carrier transport across QWs [12].

In this paper, we show experimental results in a *p-i-n* Ge/SiGe QW modulator for understanding both recovery of excitonic saturation due to intervalley scattering in the Ge QWs and carrier screening of the applied field on longer timescales. We determine the Γ to L intervalley scattering time to be ~185 fs, and show that it contributes only moderately to the exciton linewidth of the absorption spectra of the QWs. We also model the subsequent transmission changes due to field screening by carrier escape from the QWs, drift through the intrinsic region, and diffusive conduction across the doped electrodes, establishing first estimates of the timescales for these processes in Ge quantum well structures. Finally, we discuss the implications of our findings for future modulator performance and for the use of Ge/SiGe QWs as fast saturable absorbers.

2. Sample design and fabrication

All measurements were performed using a surface-normal modulator in a *p-i-n* configuration, with the QWs in the intrinsic region as shown in Fig. 1(a). The first step in fabricating this device was the epitaxial growth of the QWs on a silicon wafer by reduced pressure chemical vapor deposition at Lawrence Semiconductor Research Laboratory in Tempe, AZ. To begin, a 1 μm boron-doped $Si_{0.1}Ge_{0.9}$ buffer was grown in two stages, each followed by high temperature anneals [1]. Next, a thin 150 nm undoped layer of $Si_{0.1}Ge_{0.9}$ was grown, followed by 40 quantum wells in a superlattice of 16 nm pure Ge wells separated by 40 nm $Si_{0.16}Ge_{0.84}$ barriers [13]. Last, a second 150 nm undoped $Si_{0.1}Ge_{0.9}$ layer and a 400 nm arsenic-doped $Si_{0.1}Ge_{0.9}$ layer were grown. The QW region is designed to be strain-balanced, such that compressive strain in the Ge wells (caused by the 4.2% lattice mismatch of Si and Ge) is approximately balanced by tensile strain in the SiGe barriers.

Photodiode mesas were lithographically defined on the epitaxial surface, and samples were etched to allow contacting of the p-type layer. Anti-reflection coatings were deposited on both sides of the device and Ti/Al ring contacts were evaporated to contact both n- and p-type layers. In this work, measurements were taken on a large, 450 μm x 450 μm square mesa.

3. Experiment

To resolve the carrier dynamics of the QW structure on an ultrafast time scale, time-resolved transmission data were recorded using the collinear pump-probe setup shown in Fig. 1(b). A short-pulse fiber laser (Thorlabs FSL1010) was used with a bandwidth of ~29 nm centered at 1570 nm and a repetition rate of 79.7 MHz; the laser's broad spectrum covered the entire exciton resonance peak of the QWs. At the location of the sample, the laser pulse length was measured to be ~120 fs by autocorrelation using two-photon absorption in a commercial Si detector [14]. The experiment was performed with crossed pump and probe linear polarizations so that the transmitted pump beam could be filtered out before the final detector using a polarizing beam splitter. The use of cross-polarized beams also helped minimize any possible coherence artifact [15,16]. The two beams overlapped on the sample with a spot radius of 7.5 μm. The scanning knife-edge method was used to measure the $1/e^2$ intensity radius of the collimated beam immediately before it was focused using the 10x objective lens [17]; the focused spot size, W_0', was calculated from this incoming beam radius, W_0, using the ideal relationship $2W_0' = 4\lambda F_{\#} / \pi$, where $F_{\#} = f/2W_0$. Using this pump-probe configuration, changes in the transmission of the probe pulse induced by the pump pulse were detected as a function of the delay between the two pulses.

#136041 - $15.00 USD Received 4 Oct 2010; revised 11 Nov 2010; accepted 14 Nov 2010; published 22 Nov 2010

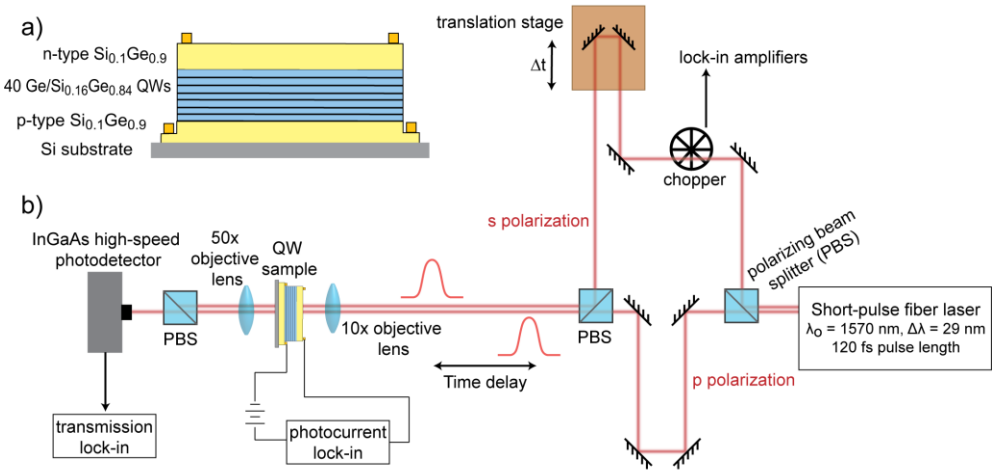

Fig. 1. (a) Diagram of the modulator used in this experiment. The device consisted of Ge/SiGe QWs in the intrinsic region of a reverse-biased *p-i-n* diode. (b) Pump-probe setup used to measure the changes in the probe transmission of the QWs. The different polarizations of the pump and probe beams allowed us to detect changes in the probe induced by the pump as a function of time delay between the two.

The QCSE is a shift of the QW absorption spectrum, including the strong excitonic peak characteristic of the QCSE, to longer wavelengths with increasing electric fields. The entire absorption spectrum can also be redshifted by heating the QWs due to a narrowing of the bandgap of the well material with increased temperature [1]. Using a combination of heating and voltage biasing, we shifted the exciton absorption peak of the QWs to maximize its overlap with the laser emission spectrum of our short-pulse fiber laser.

In the experiment to observe saturation of the exciton, the pump fluence was 61 fJ/μm^2 and the probe fluence was 3.6 fJ/μm^2. A low fluence was used to ensure that the device exciton absorption was not being heavily saturated. The observations of field screening required additional reduction of the pump fluence to 6.4 fJ/μm^2 and the probe fluence to 0.48 fJ/μm^2. Due to the QCSE, the absorption of the QWs is extremely sensitive to the applied electric field, which can be partially screened by the movement of photogenerated carriers toward the electrodes. The low fluence ensured that the change in absorption resulting from screening-induced voltage changes was linear.

4. Results and discussion

Time-resolved experiments to measure the intervalley scattering time and determine the characteristic times associated with other carrier dynamics of the QWs were carried out under a range of temperatures and applied biases, in order to understand and distinguish between the multiple effects occurring. The transmission signal that is recorded from this material can be described by two main contributions: (i) fast bleaching of the exciton, exhibited by a rapid increase in the transmission signal and a subsequent rapid recovery that is, presumably, primarily due to intervalley scattering, and (ii) subsequent screening of the applied field as the electrons and/or holes move out of the quantum wells toward the electrodes of the diode structure. Due to field screening, we expect a consequent temporary reduction in the voltage across the quantum wells in the region of the laser spot, causing a blue shift of the exciton peak, followed by recovery of the voltage back to a uniform equilibrium value by diffusive conduction in the diode electrodes [10,12]. Because of our deliberately low fluences in the experiments, the total fractional change of transmission through the sample is a linear sum of changes from saturation of the absorption, $H_{sat}(t)$, and field screening, $H_{scr}(t)$:

#136041 - $15.00 USD Received 4 Oct 2010; revised 11 Nov 2010; accepted 14 Nov 2010; published 22 Nov 2010

$$\Delta T \propto C_{sat} H_{sat}(t) + C_{scr} H_{scr}(t) \quad (1)$$

where C_{sat} and C_{scr} are proportionality constants [12].

4.1 Fast absorption saturation

$H_{sat}(t)$ is the time response of the optical saturation at a time t following the excitation pulse. Figure 2 shows an example of the time-resolved pump-probe data we obtain. (Here and in Fig. 4, rapid fringes due to interference on the photodetector between the transmitted probe and any pump signal that leaked through the polarizing beam splitter have been smoothed by filtering of the data. Data points dropped by the lock-in amplifier used to record data have also been omitted.) Around the point of zero delay between the pump and probe pulses, we see a strong bleaching followed by a fast recovery. We presume that the dominant absorption change on this sub-picosecond timescale is due to bleaching associated with the electrons occupying the direct Γ conduction band valley, with a corresponding rapid recovery due to those excited electrons scattering to the lower energy, indirect L valley [5,6]. Occupation of the zone center valence band states may also contribute to the saturation of the exciton but, because of the relatively large heavy hole effective mass and the resulting large density of states, this is expected to be a smaller effect [6]. This conduction band intervalley scattering is seen in bulk Ge, where it has been ascribed to deformation potential phonon scattering, the major scattering mechanism in non-polar materials [5,7,15].

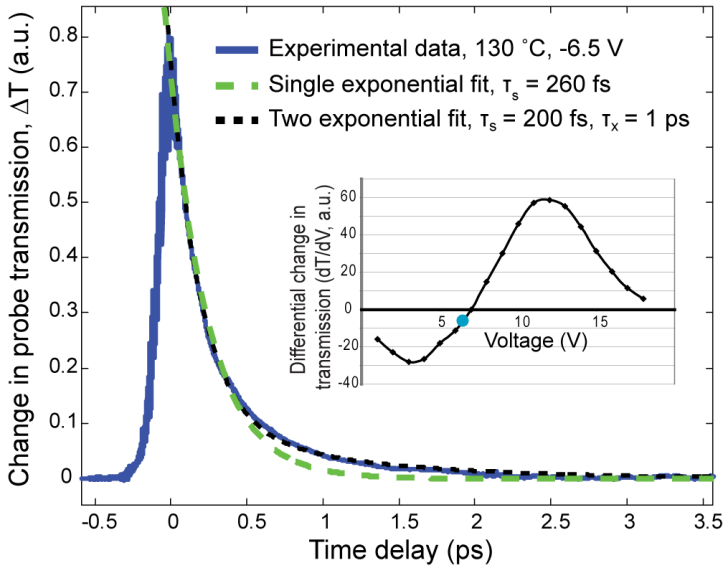

Fig. 2. Change in transmission of the probe pulse as a function of its time delay relative to the pump pulse. Dashed curve – fit to a single exponential. Dotted curve – fit to the sum of two exponentials. The single exponential (260 fs) or the faster exponential (200 fs) in the two exponential fit is presumed to be from intervalley scattering in the conduction band. The addition of the slower exponential allows a better fit; speculatively, it might be due to hole scattering or escape. The inset of the figure shows the changes that occur in transmission at 130 °C with small changes in voltage. The large dot indicates the voltage at which this data was taken, where we expect very small changes in transmission with changes in voltage.

The combination of heating the sample to ~130 °C and applying 6.5 V reverse bias to obtain the data in Fig. 2 was chosen because, under these conditions, there is no net effect of the field screening on the optical absorption—the change in absorption with voltage is negligible in the immediate vicinity of this particular operating point. This can be seen in the inset of Fig. 2, which shows differential changes in transmission as a function of small changes in voltage. At 6.5 V, there is a relatively small change in transmission with a small

#136041 - $15.00 USD Received 4 Oct 2010; revised 11 Nov 2010; accepted 14 Nov 2010; published 22 Nov 2010

change in voltage. Hence, the transmission recovers to a value very close to what it was before the zero time delay point and stays relatively constant thereafter, allowing the bleaching recovery to be separated from field screening effects. The saturation is initially modeled with a simple exponential time dependence for short times after zero delay, with a characteristic time decay, τ_s, which we associate with the intervalley scattering of the electrons [12]:

$$H_{sat}(t) = e^{-t/\tau_s}. \quad (2)$$

The signal in Fig. 2 was fitted with τ_s equal to 260 fs (dashed line). The detected optical response is a convolution of the exciton saturation signal and the finite excitation pump pulse (~120 fs pulse width). Using the model in [18], the pump pulse length was deconvolved from the signal and the actual scattering time deduced to be ~250 fs. Though a single exponential recovery models the main behavior of this saturation recovery moderately well, there is a noticeable discrepancy between ~0.5 and 2 ps delay. To remove this discrepancy, we found that the sum of two exponential decays gave a better fit to this data (dotted line), one with a fast decay time of τ_s = 200 fs and the second with a slower decay time of τ_x = 1 ps. For τ_s = 200 fs, the scattering time was deconvolved to be ~185 fs. We postulate that the second, slower exponential could be due to some small additional bleaching recovery from a process associated with holes scattering to other states and/or escaping from the wells. Light holes in particular are known to be only very weakly bound to the wells in the presence of even moderate field [13]. Initial observations show that the value of this second exponential time remains approximately constant as the electric field applied across the *p-i-n* diode increases, leading us to the conclusion that the magnitude of this secondary bleaching is not field-dependent.

This 185 fs scattering time—which can be directly related to the exciton lifetime—is too long to contribute significantly to the linewidth of the exciton peak observed in the absorption spectra of these QWs through homogenous broadening [19]. Using a simple Lorentzian peak model to relate the half width at half maximum of the peak, HWHM, to the exciton lifetime, Δt, gives $HWHM = \hbar/(2\Delta t)$. Based on the 185 fs scattering time measured here, the half-width at half-maximum, HWHM, of the exciton is predicted to be 1.8 meV. The lowest exciton HWHM we have measured is 6.25 meV [20]; other work has reported a HWHM of the exciton in similar structures to be 6 meV [21]. The 1.8 meV calculated here presents a lower bound for exciton widths in this material system; the fact that grown samples have much larger widths suggests that other factors associated with the structure of the QWs are contributing significantly to a broadening of the exciton peak. Specifically, this inhomogeneous broadening can occur through fluctuations of the confinement energies of carriers in the wells due to variations in layer thicknesses [19] or unwanted doping in the intrinsic region resulting in a non-uniform electric field across the QWs [22]. Based on a simple Bose-Einstein distribution for the number of phonons in the necessary modes, we expect the dominant scattering is phonon emission rather than absorption even at room temperature or somewhat higher [5], so we do not expect strong temperature dependence. Experimentally we have observed an increase in the exciton HWHM of less than 1 meV as a 60 QW sample is heated from 30 °C to 100 °C [22], though it is unclear whether this broadening is due to phonon-related effects or other temperature-dependent changes.

4.2 Saturation fluence

Ge/SiGe quantum wells hold promise as fast saturable absorbers for laser modelocking due to the rapid recovery of their absorption saturation. Germanium has previously been used as a saturable absorber [23] for a solid state laser. In that prior work, the fast saturation recovery was attributed to intervalley scattering, a feature we expect could also be exploited when using Ge QWs. To determine the saturation fluence in our case, the change in absorption of the QWs was measured as a function of average beam power. In this experiment, the pump

#136041 - $15.00 USD Received 4 Oct 2010; revised 11 Nov 2010; accepted 14 Nov 2010; published 22 Nov 2010

and probe beam pulses arrived at the same time on the sample, only the probe beam was chopped, and the resulting photocurrent associated with probe beam absorption was detected using a lock-in amplifier. This probe beam photocurrent was recorded as the pump beam fluence was changed (the probe beam fluence was simultaneously changed by an equal percentage). The pump beam fluence, J_o, at the center of the Gaussian-shaped pump beam was calculated from this measured average power and is plotted in Fig. 3 versus change in absorption. The change in absorption was determined from the ratio of the photocurrent when the pump beam was absorbed by the sample (possibly bleaching its absorption of the probe beam) to the photocurrent when the pump beam was blocked; this ratio is expected to be less than 1 if any saturation is occurring. This data was taken at 100 °C with 15.5 V applied across the sample, conditions that were determined to allow the most overlap of the laser spectrum and the absorption spectrum of the QW exciton peak.

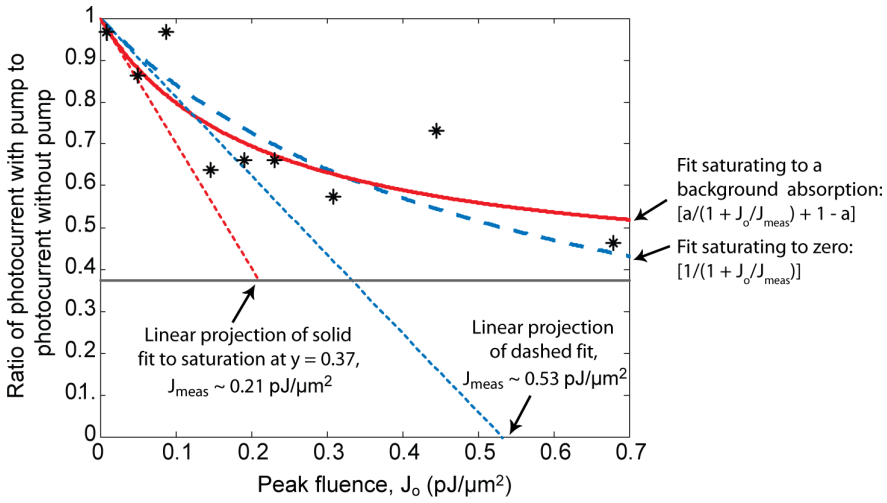

Fig. 3. By taking the ratio of probe beam photocurrent with and without the pump beam, saturation of the absorption of the QWs is evident in the experimental data points shown. From this data, recorded at 100 °C and 15.5 V reverse bias, we estimate the saturation fluence to be between 0.11 and 0.27 pJ / μm^2. The dashed line is a fit of the general form of $[1/(1 + J_o/J_{meas})]$, saturating to zero absorption; the solid line is a fit of the general form $[a/(1 + J_o/J_{meas})] + 1 - a$, provided to show the general trend of the data saturating to an apparent non-zero background absorption at $1 - a = 0.37$ (grey horizontal line). The dotted lines show the linear projection of these fits at low fluences. The actual saturation fluence after deconvolving the effect of the Gaussian beam shape is $J_{meas}/2$ in each case as discussed in the text.

A commonly-used simple microscopic saturation model of absorption, A, as a function of fluence, J, is $A/A_o = 1/(1 + J/J_{sat})$, where A_o is the absorption at very low fluence. For small fluences this can be written approximately as $A/A_o = 1\text{-}J/J_{sat}$, which means that the tangent to the saturation curve at low fluences intercepts the horizontal axis at a value J_{sat}. We begin by fitting our experimental data of Fig. 3. The dashed fit has the form, $1/(1 + J_o/J_{meas})$, and saturates to zero at large peak fluences with $J_{meas} = 0.53$ pJ/μm^2. However, because many mechanisms can be involved in absorption saturation in semiconductors, we need to consider also the possibility that this particular absorption saturation saturates to a non-zero background absorption. To account for this, we compare with a second fit of the form $[a/(1 + J_o/J_{meas})] + 1 - a$, shown by the solid line in Fig. 3, which we fit to saturate to a background of $1 - a = 0.37$, and which then has $J_{meas} = 0.21$ pJ/μm^2 .

To accurately determine a microscopic J_{sat}, we need to deconvolve the effect of the Gaussian beam, whose local fluence varies with radius r according to $J(r) = J_o \exp(-2r^2 / w_o^2)$. This deconvolution is relatively straightforward when we are in the

#136041 - $15.00 USD Received 4 Oct 2010; revised 11 Nov 2010; accepted 14 Nov 2010; published 22 Nov 2010

approximately linear regime of saturation at low fluences. In that regime, the total measured photocurrent I_{tot} will be

$$I_{tot} \propto \int_{r=0}^{\infty} J(r) A_0 \left(1 - \frac{J(r)}{J_{sat}}\right) 2\pi r dr \qquad (3)$$

From Eq. (3), we find that this initial linear decrease is of the form $I_{tot} / J_o \propto (1 - J_o / 2J_{sat})$. This means that the effective average fluence in the Gaussian beam for the purposes of this simple saturation model is half the peak fluence.

Thus, J_{sat} is effectively half of the value for J_{meas} found by the linear extraction method explained above and shown in Fig. 3. If we assume $A(r)/A_o$ saturates to zero, J_{sat} = 0.27 pJ/μm^2; if we use the model that assumes some non-saturable background absorption and allow $A(r)/A_o$ to saturate at a non-zero value, J_{sat} = 0.11 pJ/μm^2. Hence, we have established a range of possible values based on two reasonable simple models of the absorption saturation and accounting for the Gaussian distribution of fluences in the beam area.

The range of possible saturation fluences found here is slightly less than that observed (0.3 pJ/μm^2) by Grawert *et al.* [23] in bulk germanium, despite the fact that the quantum well is under strong bias in these measurements (because such bias reduces the electron-hole overlap through the QCSE, leading to reduced absorption, it could be expected that the saturation fluence would increase). Quantum wells in other materials, however, are known to possess particularly strong saturation effects when compared to bulk materials, which makes them attractive for mode-lockers [24].

Both the quantum wells and the bulk germanium have the feature that they can be fabricated together with Si/SiO_2 mirror stacks [20] that can offer very high reflectivites with small numbers of layer pairs. Such mirrors are required for saturable Bragg reflector [23] or related semiconductor saturable absorber mirror [25] configurations. The fact that the excitonic absorption can be spectrally tuned in the quantum well through the QCSE adds another degree of freedom for use as a saturable absorber. The ability to control the absorption with an electric field opens possibilities for combined active/passive modelocking. Additionally, field screening effects may allow induced absorption after the initial saturation, a phenomenon that can suppress undesired Q-switching in a laser (see the discussion in [23]). Our field screening results shown explicitly in Fig. 4 below are taken under conditions that lead to increased transmission, but other temperature and bias voltages (e.g., 130 °C, > 7 V, or 100 °C, > 15 V) can show temporary induced absorption, due to the increase in absorption as the voltage is reduced under some combinations of wavelength and bias.

4.3 Field screening and diffusive conduction

The field screening function, $H_{scr}(t)$, is proportional to the change in the average electric field applied to the QWs for suitably small changes in field or voltage. Field screening occurs because the photogenerated carriers from the pump pulse absorption leave the wells and transport to the biasing electrodes, reducing the voltage locally on the diode. Due to the dependence of the QW absorption on the effective applied electric field, we observe that the sign and shape of the field screening signals seen in transmission measurements vary at times longer than ~1 ps, depending on the temperature and bias applied to the device. This can be seen from the differential changes in transmission with voltage that are shown in the insets of Fig. 2 and 4, where the magnitude and sign of the signal depends on both voltage and temperature. These changes are consistent with the QCSE: field screening effectively decreases the voltage applied across the QWs. For biases where the exciton peak is at wavelengths longer than the laser spectrum, absorption increases with a decrease in electric field as the exciton peak shifts to lower wavelengths, increasing its overlap with the laser spectrum. However, for biases where the exciton peak overlaps in wavelength with the laser spectrum or is at slightly lower wavelengths, field screening decreases the absorption of the

#136041 - $15.00 USD Received 4 Oct 2010; revised 11 Nov 2010; accepted 14 Nov 2010; published 22 Nov 2010

QWs. Figure 4 shows experimental data taken over more than 100 ps. Each of the mechanisms of interest to this work can be seen: the intervalley scattering discussed above, which appears as a sharp spike in the transmission with a subsequent fast recovery, followed by the onset of field screening 3-20 ps after the zero delay point as the carriers begin to move towards the contacts, and finally the dominance of diffusive conduction after about 20 ps as the device returns to its initial state, settling completely ~120 ps after the arrival of the pump pulse. This data was taken at 100 °C and 8 V reverse bias, with the consequence that the exciton absorption peak is at slightly lower wavelengths than the laser spectrum. This set of experimental conditions was chosen because empirical observations suggest that it is here that the total power absorbed from the laser varies approximately linearly with electric field. This data is shown in the inset of Fig. 4, where around 8 V (indicated by the large dot), the differential change in transmission at different voltages is nearly constant (which corresponds to a linear change in actual transmission with changes in electric field).

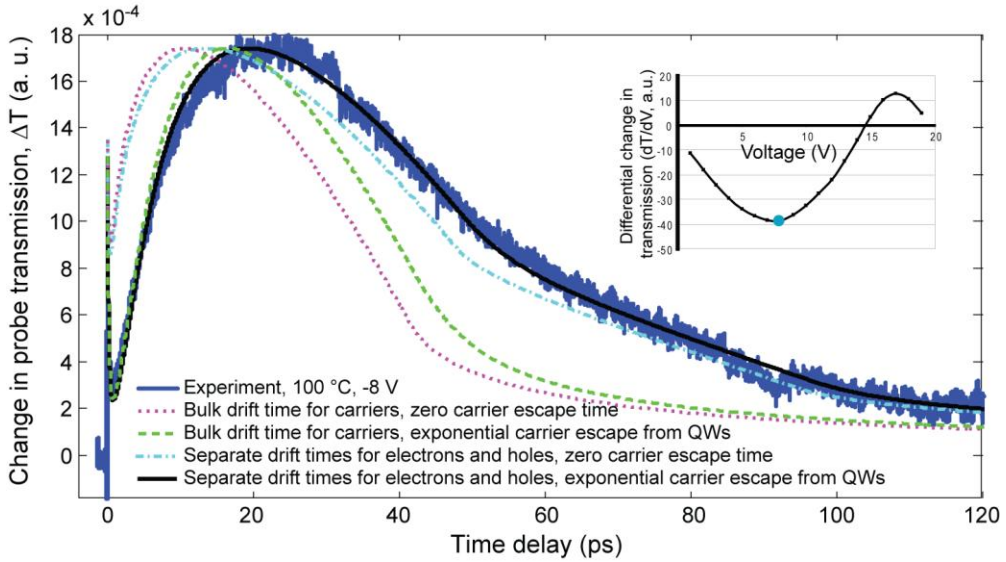

Fig. 4. Field screening is observed in the transmission of the QWs at times following the fast excitonic saturation. A model incorporating the carrier drift time and diffusive conduction (the dotted line is calculated using an estimated drift time for both holes and electrons of 42 ps) can be improved by including separate drift times for each carrier type of 48 and 96 ps (dot-dashed line) or by including a finite exponential time constant of 4 ps (dashed line) for carriers to escape from the QWs. The best fit is achieved by incorporating both improvements (solid line).

5. Modeling of field screening

To better model the field screening that occurs following excitation of the carriers in the QWs, three transport mechanisms need to be considered: 1) the escape of the carriers from the wells; 2) the drift of the carriers through the intrinsic region to the contacts; and 3) diffusive conduction [10,12]. Diffusive conduction is the process of conduction in the p and n doped regions by which any lateral voltage non-uniformities across the doped regions relax. For example, following excitation of photocarriers in the diode by, say, a Gaussian-shaped laser spot, the vertical separation of the photogenerated-charges will tend to lead to a Gaussian-shaped reduction in the voltage, distributed laterally across the doped regions and centered at the middle of the laser spot. Since the diode's p and n doped regions are conducting, such a non-uniform voltage is not stable. The process by which this lateral voltage distribution relaxes across the contacts can be described by a diffusion-like equation. It is, however, important to emphasize that this diffusion is a voltage diffusion that can be understood simply from resistance and capacitance in the diode [10,11]; it is not (directly) the lateral diffusion of

#136041 - $15.00 USD Received 4 Oct 2010; revised 11 Nov 2010; accepted 14 Nov 2010; published 22 Nov 2010

the photogenerated carriers themselves across the doped regions. Indeed, this process can be much faster than the direct diffusion of carriers in the semiconductor [11]. $H_{scr}(t)$ is the convolution of the impulse responses from carrier escape from the quantum wells, $g_1(t)$, carrier drift through the intrinsic region, $g_2(t)$, and the diffusive conduction, $g_3(t)$. Of these three processes, the carrier drift and diffusive conduction can be estimated analytically, while less is understood about the carrier escape time from the QWs.

Considering the drift of the carriers generated at all the different points in the quantum well region, the overall drift process leads to a driving term, $g_2(t)$, for the diffusive conduction that is essentially triangular in time. Initially, all the carriers that escape from the wells at some time $t = 0$ start to move "vertically" in the diode toward the p or n doped regions, leading to a step-like rise in $g_2(t)$. As the carriers reach the electrodes, they no longer contribute to driving the diffusive conduction; thus, the drive decays linearly in time as the carriers from different depths in the diode reach the electrodes. The width of this triangular current pulse is therefore of duration equal to the time required for a carrier to cross the Ge-rich, 2.5 μm-thick intrinsic region. We presume that the carriers are likely to move at a velocity of the same overall scale as the saturated drift velocity for carriers in Ge (~6 x 10^6 cm/s for both electrons and holes at ~100 °C [26]). Such a drift velocity would result in an estimated minimum drift time for the carriers generated furthest away from their destination electrode of 42 ps. In our case here, the carriers have to transport across the quantum wells. For the electrons in particular, where the conduction band structure changes substantially between the wells and the barriers, we might expect a different behavior, possibly leading to a slower effective drift velocity. To account for possible differences in the transport mechanisms of electrons and holes, we included two separate triangular drift impulse responses, one for each type of carrier. In addition to these two triangles, we also add a "spike" to $g_2(t)$ at the time of optical absorption because the electron-hole pairs are created already polarized by the applied electric field. The magnitude of this spike and the height of the two triangular current pulses were calculated by modeling the photocarriers generated in the QWs as charges on parallel plate capacitors.

The response due to diffusive conduction, $g_3(t)$, is more complex. As mentioned above, diffusive conduction occurs when light is absorbed in the intrinsic region of the structure and the photogenerated carriers move toward the contacts, separating and creating a lateral voltage distribution in the shape of the optical beam [10]. The voltage distribution then relaxes laterally by conduction in the electrodes, governed by a diffusion-like equation:

$$\partial V(x,y,t)/\partial t = D\nabla^2 V(x,y,t) \tag{4}$$

where $D = 1/R_{sq}C_A$, with C_A being the capacitance per unit area of the device and R_{sq} being the sum of the sheet resistances (in Ω/sq.) of the p and n layers. Based on our presumed material properties, including our expected resistivities of the ~5×10^{17} - 1×10^{18} cm^{-3} doped n and the ~3×10^{17} - 1×10^{18} cm^{-3} doped p regions, we estimate D to be in the range of 15 - 45 m^2/s. (Dopant densities were estimated from the secondary ion mass spectrometry (SIMS) data of similarly-grown samples.) For a Gaussian shaped beam and a finite, circularly-shaped mesa of radius, R, with an initial condition of $V = f(r) = \exp(-2r^2/\omega_0^2)$ (ω_0 equal to the radius of the spot on the mesa), and a boundary condition at the mesa edge of $\partial V/\partial r = 0$, the solution to Eq. (4) is

$$g_3(t) = V(r,t) = \int_0^R f(\xi) G(r,\xi,t) d\xi \tag{5}$$

$$G(r,\xi,t) = \frac{2}{R^2}\xi + \frac{2}{R^2}\sum_{n=1}^{\infty} \frac{\xi}{J_0^2(\mu_n)} J_0\left(\frac{\mu_n r}{R}\right) J_0\left(\frac{\mu_n \xi}{R}\right) e^{-\frac{D\mu_n^2 t}{R^2}} \tag{6}$$

#136041 - $15.00 USD Received 4 Oct 2010; revised 11 Nov 2010; accepted 14 Nov 2010; published 22 Nov 2010

where μ_n are positive zeros of the first-order Bessel function. This particular boundary condition is appropriate if no charge flows off the edge of the mesa during the timescale of interest; nearly identical simulation results are obtained for our device if instead we assume that the voltage is held constant at the edge of the mesa during the experiment, reflecting the fact that the overall possible voltage change over the mesa is relatively negligible here because the mesa is much larger than the laser spot. We note that we have used a circular form for our mesa in the simulations for simplicity even though the mesa itself is square; again, because of the large size of the mesa compared to the laser spot size, we expect negligible error from this simplification at short times.

Figure 4 shows the fits that result from the above model. The dotted line shows the fit using only a single triangle to model the drift of both carriers, with a length equal to the estimated drift time of 42 ps and D = 30 m^2/s; in this particular fit, the carrier escape time from the QWs was presumed to be zero to show the simplest possible model. A better fit can be achieved by including a 4 ps exponential time constant for both the electrons and holes to escape from the QWs (dashed line). The original fit can also be improved by incorporating two drift rates for the two different particles (electrons and holes), one with a slightly longer carrier drift time of 48 ps than the estimate from bulk Ge behavior and the second with a significantly longer time of 96 ps (dot-dashed line); carrier escape was again assumed to be zero in this dot-dashed curve for comparison purposes. Finally, the best fit can be achieved by combining both the two drift rates of differing lengths for each carrier type and the finite carrier escape lifetime (solid line). It should also be noted that using any D within the range of 15 - 45 m^2/s calculated above provides very similar results over the timescale in Fig. 4; the drift times used to achieve the best fits for these different D values need to be changed by at most 5 ps from those reported here.

As indicated by the solid fit in Fig. 4, by including both separate drift impulse responses for electrons and holes and a finite carrier escape time from the QWs, the model matches the data extremely well across the entire time range. One important finding from our model is the longer drift times that are required to accurately fit the experimental data. One explanation is that, as the carriers travel across the intrinsic region, rather than drifting continuously as would occur in bulk Ge, they may be recaptured and emitted from the QWs that they pass through. This would most likely affect electrons and holes differently, since each carrier faces different energy barriers between each QW, and would thus result in the need for the separate drift triangular impulse responses for each carrier type. Another interesting point is that we do not need to assume different escape times for the electrons and holes to fit the data here. This is not an expected result, again due to the different energy barriers faced by the carriers. It is possible that some more sophisticated model could be constructed but, in the absence of any microscopic model, we would not be justified in increasing the number of adjustable parameters in our fit.

6. Conclusion

Ge/SiGe quantum well modulators are promising components for future optical interconnects. In this work, we investigated the carrier dynamics and transport properties of Ge QW structures, in order to gain a better understanding of their device performance potential and limitations. We focused on two time-regimes: the ultrafast intervalley scattering in Ge that occurs in hundreds of femtoseconds, and the subsequent field screening and its recovery via diffusive conduction as the carriers drift through the intrinsic region in hundreds of picoseconds.

We determined the intervalley scattering time of electrons in the conduction band from the direct Γ valley to the indirect L valley of Ge wells to be ~185 fs. We observed a second exponential process that decays in ~1 ps, which could be associated with saturation due to holes and subsequent hole scattering or escape, though our experiments do not allow more detailed conclusions. The exciton absorption peak width observed experimentally is much

#136041 - $15.00 USD Received 4 Oct 2010; revised 11 Nov 2010; accepted 14 Nov 2010; published 22 Nov 2010

larger than the lower bound set by this short lifetime, which suggests that much of the remaining broadening results from nonidealities in the QW growth. Due to the fast recovery of the exciton bleaching, Ge/SiGe QWs could be used as a saturable absorber in future mode-locked lasers. The saturation fluence was estimated to be between 0.11 and 0.27 $pJ/\mu m^2$.

Following the fast exponential decay that occurs primarily through intervalley scattering, field screening occurs. To accurately model this, we combined the effects of carrier escape time from the QWs, the time it takes the carriers to drift across the device, and the recovery of the applied voltage through diffusive conduction. We see evidence suggesting the carriers may take a short time (~4 ps) to be emitted from the wells, as well as evidence of the electrons and holes transporting with somewhat different effective saturated drift velocities through the structure. The device recovers fully within 120 ps, indicating that, though the intervalley scattering time is extremely fast and represents a fundamental limitation of the speed of the QCSE in our modulators in the THz range, the actual limitation comes about from the time it takes for the device to completely recover via diffusive conduction. This recovery time could be shortened (effectively decreasing the *RC* constant of our device) by increasing the dopings of the n and p regions, decreasing device size, and decreasing the device capacitance.

Acknowledgments

This work was supported in part by Oracle under contract HR0011-08-9-0001 between the Government and Oracle. The views, opinions, and/or findings contained in this article are those of the authors and should not be interpreted as representing the official views or policies, either expressed or implied, of the Defense Advanced Research Projects Agency or the Department of Defense. The authors also acknowledge the support of the IFC Focus Center, one of six research centers funded under the Focus Center Research Program, a Semiconductor Research Corporation program. Emel Tasyurek acknowledges the support of a Stanford Graduate Fellowship and Stephanie Claussen acknowledges the support of a National Science Foundation Graduate Research Fellowship. Work was performed in part at the Stanford Nanofabrication Facility (a member of the National Nanotechnology Infrastructure Network) which is supported by the National Science Foundation under Grant ECS-9731293, its lab members, and the industrial members of the Stanford Center for Integrated Systems.

#136041 - $15.00 USD Received 4 Oct 2010; revised 11 Nov 2010; accepted 14 Nov 2010; published 22 Nov 2010